# Tailoring the topological surface state in thin $\alpha$-Sn films

V. A. Rogalev,[1] F. Reis,[1] F. Adler,[1] M. Bauernfeind,[1] J. Erhardt,[1] M. R. Scholz,[1] L. Dudy,[1]
L. B. Duffy,[2] T. Hesjedal,[2] M. Hoesch,[3] G. Bihlmayer,[4] J. Schäfer,[1] and R. Claessen[1]

[1] *Physikalisches Institut and Würzburg-Dresden Cluster of Excellence ct.qmat, Universität Würzburg, 97074 Würzburg, Germany*
[2] *Clarendon Laboratory, Physics Department, Oxford University, OX1 3PU, United Kingdom*
[3] *Diamond Light Source, Didcot, OX11 0DE, United Kingdom*
[4] *Peter Grünberg Institut, Forschungszentrum Jülich and JARA, 52425 Jülich, Germany*

(Dated: October 7, 2019)

We report on the electronic structure of $\alpha$-Sn films in the low thickness regime grown on InSb(111)A. High-resolution angle-resolved photoemission (ARPES), enhanced at low photon energies, allows for the direct observation of the linearly dispersing 2D topological surface states (TSSs) that exist between the second valence band and the conduction band. The Dirac point of this TSS was found to be 200 meV below the Fermi level in 10-nm-thick films, which enables the observation of the hybridization gap opening at the Dirac point of the TSS for thinner films. The cross-over to a quasi-2D electronic structure is accompanied by a full gap opening at the Brillouin zone center, in agreement with our density functional theory calculations. We further identify the thickness regime of $\alpha$-Sn films where the hybridization gap in TSS coexists with the topologically non-trivial electronic structure which must result in a presence of 1D helical edge states.

## I. INTRODUCTION

The low temperature $\alpha$-phase of Sn belongs to a family of materials with a topologically non-trivial electronic band structure [1]. Due to its mono-elemental nature, and the resulting favorable defect chemistry, $\alpha$-Sn has recently attracted considerable interest [2–7]. In particular, $\alpha$-Sn thin films grown by molecular beam epitaxy (MBE) exhibit outstanding quality [4, 7, 8]. In contrast to $Bi_2X_3$ compounds (X = Se or Te), band inversion in bulk $\alpha$-Sn involves the *second* valence band (VB) $\Gamma_7^-$ and conduction band (CB) $\Gamma_8^+$, which reveal $s$-like and $p$-like character, respectively [9]. Such band order is also typical of HgTe [10, 11] and some half-Heusler compounds [12] and results in fact in a double band inversion with a pair of TSSs of different wavefunction localization character [5]. Most of the substrates available for epitaxial growth provide an in-plane compressive strain for $\alpha$-Sn films, which drives them into a Dirac semimetal phase [5, 13] with both TSSs being fully degenerate with bulk states. Yet, previous studies on in-plane compressively strained $\alpha$-Sn thin films revealed that the hybridization between the upper TSS, in focus of the present work, and the bulk states is weak due to differences in the orbital composition [5, 14]. This allows for the observation of a sharp $E(\vec{k})$ dispersion of this TSS in spin- and angle-resolved photoemission (ARPES).

The (111) surface of $\alpha$-Sn is of particular interest due to its close relationship to the family of 2D honeycomb lattices in group IV high-$Z$ materials, e.g., stanene, bismuthene and antimonene. These have been widely investigated, both theoretically and experimentally, as a new platform for utilizing helical spin-polarized topological edge states [15]. Despite numerous reports on the fabrication of stanene on a variety of substrates [16–22], the study of the 3D to 2D transition of the TSS in $\alpha$-Sn films has remained scarce. With the reduced thickness, the 3D bulk band structure changes developing gap(s) due to increasing confinement in a quantum well and the surface- and interface-TSSs (at the $\alpha$-Sn/substrate interface) wavefunctions start to overlap. Similar to HgTe/CdTe quantum wells [23, 24], the bulk band inversion in $\alpha$-Sn can be lost at some certain critical thickness [25–27] or even show an oscillatory behavior [28] depending on thickness. Additionally, given the band inversion remains, the hybridization between surface- and interface-TSSs in thin $\alpha$-Sn films could open a gap at the Dirac point (DP). In such case the system can be classified as a 2D quantum spin Hall insulator (QSHI) with 1D helical edge states.

In this paper we report on the electronic structure of thin $\alpha$-Sn films epitaxially grown on InSb(111)A, and, in particular, on the evolution of the TSS as a function of thickness exploiting high-resolution ARPES and density functional theory (DFT) calculations which notably include the substrate. We find that, in contrast to $\alpha$-Sn on InSb(001), the DP of TSS for the (111) surface orientation is situated significantly below the Fermi energy for 10 nm-thick $\alpha$-Sn films. The latter enables the direct observation of the hybridization gap opening at the DP for thinner films. Thus, for a 3-nm-thick film we find a gap in the TSS of the order of $\Delta E^g_{peak} \approx 200$ meV (peak-to-peak). The electronic structure of the quasi-2D 1-nm-thick films exhibits a full gap opening at the $\Gamma$-point ($\Delta E^g_{peak} \approx 400$ meV). Our DFT calculations for thin $\alpha$-Sn films on InSb(111)A show good agreement with the experimental data, as well as provide evidence for the spin-polarized character of the TSS. Furthermore, we establish that coexistence of the TSS hybridization gap and the topologically non-trivial bandstructure appears in a narrow $\alpha$-Sn films thickness range of $\sim$ 2 - 10 nm, which must result in a presence of a 1D helical edge states. In addition, we report on a new (8×8) surface reconstruction observed in low-energy electron diffraction (LEED)

and scanning tunneling microscopy (STM).

## II. METHODS

$\alpha$-Sn thin films were grown by MBE on $n$-doped In-terminated InSb(111) substrates. The 8-effusion cell MBE system is directly attached to the high-resolution ARPES system at beamline I05 at the Diamond Light Source (Didcot, UK), allowing for in-vacuum transfers [29]. The substrates were cleaned by several Ar ions sputter and anneal cycles until a clear (2×2)-reconstruction was observed by LEED [see Fig. 1(a)]. During thin film growth, the InSb(111) substrates were held at ambient temperature and the $\alpha$-Sn film quality was monitored by reflection high-energy electron diffraction (RHEED). The thickness of the Sn layers was varied by changing the deposition time while keeping the flux from the effusion cell constant.

ARPES measurements have been carried out with $s$ and $p$ linearly polarized light, as well as circularly polarized light, at varying photon energies at beamline I05. The endstation is equipped with a Scienta R4000 hemispherical electron analyzer that provides an ultimate energy and angular resolution of $\sim 5$ meV and 0.1°, respectively.

STM experiments were performed with an Omicron LT-STM at a base pressure $p < 5\times10^{-11}$ mbar ($T$=4 K) using tungsten tips tested on a Ag(111) single crystal for sharpness and spectroscopic properties.

For the DFT calculations we used the full-potential linearized augmented plane wave method [30] as implemented in the FLEUR code. We employed the local density approximation to the exchange-correlation potential [31]. Our models for the 0.7 nm and 2.5 nm Sn films included four InSb(111)A substrate layers that were charge-compensated on both sides by +/- 0.25 electronic charges in the virtual crystal approximation to simulate a flat profile of the band-edges. The 7.5 nm film was calculated without substrate and in all cases hydrogen was deposited on the upper and lower surface of the film to saturate dangling bonds. To achieve a correct band-ordering we applied the DFT+U scheme as described in Ref.[2]. The same correction was applied to InSb, where the band gap is also underestimated in DFT. The films were relaxed and spin-orbit coupling was applied in a self-consistent manner [32].

## III. EXPERIMENTAL RESULTS

During growth, RHEED reveals a well-resolved 6-fold streak pattern consistent with the substrate symmetry, thus confirming the epitaxial growth of $\alpha$-Sn films on InSb(111)A substrate. However, in LEED, apart from the main (1×1) pattern, as-grown $\alpha$-Sn films show additional spots stemming from the surface reconstruction: instead of the commonly observed (3×3) surface reconstruction, we find a higher-order reconstruction [Fig. 1(b)]. Spot-profile analysis LEED (SPA-LEED) allowed to establish a (8×8) surface reconstruction [Fig. 1(c)] . The latter persists when mildly annealing the sample at $T \approx 150$ °C, leading to sharper LEED and ARPES signals. When the annealing temperature is increased further, the LEED pattern changes to the (1×1) reconstruction, in agreement with other studies [33, 34]. In addition, we performed STM measurements of 10 nm-thick $\alpha$-Sn films, which are summarized in Figs. 1(d-f). The STM measurements reveal domains with a shape close to hexagonal, which could result from twinning, i.e, an overlap of two 60°-rotated triangular domains. Twinning was indeed reported for $\alpha$-Sn films on $Hg_{0.8}Cd_{0.2}Te$(111) substrates [35]. The lateral size of domains ranges from 7× to 8× lattice constant of unstrained $\alpha$-Sn ($a$ = 4.59 Å). The step height $h \approx 3.6$ Å is consistent with the interplanar distance of $\alpha$-Sn(111) films of 3.75 Å. To the best of our knowledge, the (8×8) surface reconstruction was not reported for $\alpha$-Sn films so far. Additional STM/STS measurements are necessary to establish the exact structural model of this reconstruc-

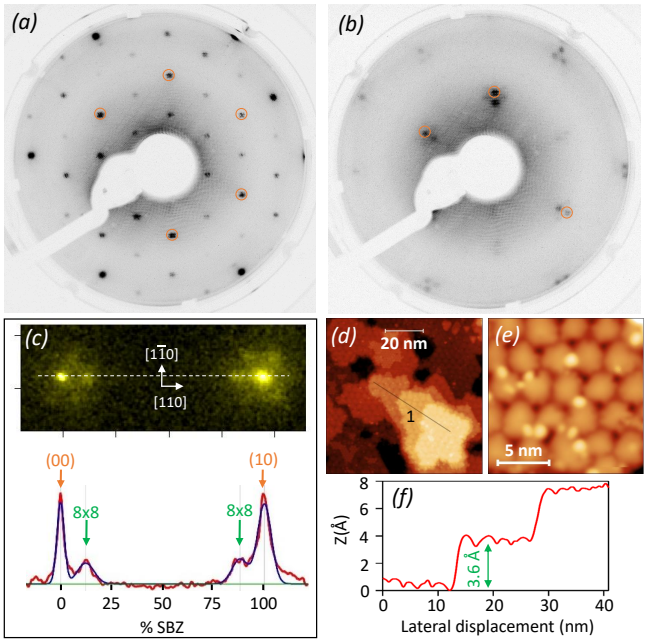


FIG. 1. (a) LEED taken at $E$=45 eV on a clean InSb(111)A substrate exhibits (2×2) surface reconstruction (orange circles denote (1×1) spots). (b) LEED taken at $E$=45 eV on 10 nm-thick $\alpha$-Sn(111) film. Apart from the expected (1×1) structure (orange circles), additional spots of high-order surface reconstruction are observed. (c) SPA-LEED data taken at $E$=87 eV and corresponding line profile (data plotted in red, 4-peaks fit - in blue) through (00) and (10) spots allow to assign the new surface reconstruction to be (8×8). (d) STM data measured with $U$=2 V, $I$=50 pA at $T$=4 K. (e) STM data on smaller scale showing domains. (f) The height profile along path labeled '1' in (d) reveals a step height of 3.6 Å.

tion.

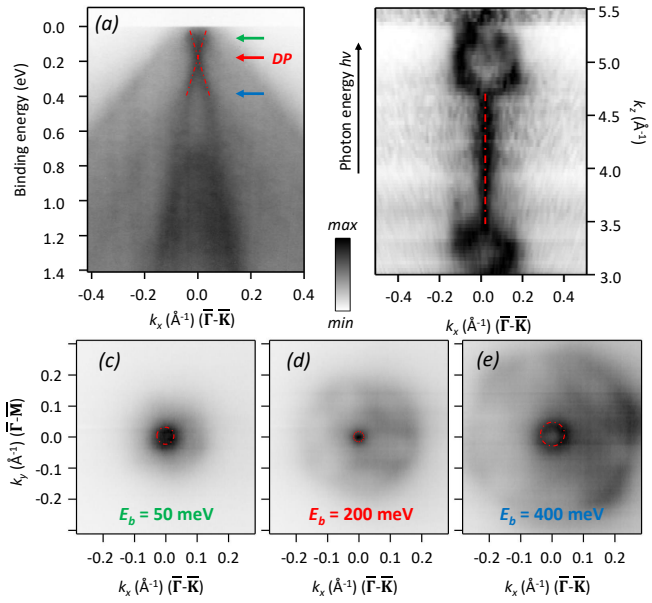


FIG. 2. Experimental electronic structure of a 10 nm-thick $\alpha$-Sn film on InSb(111)A. (a) Band map measured at a photon energy of $h\nu$ = 18 eV and at $T$ = 8 K along the $\overline{\Gamma}$-$\overline{K}$ direction. (b) Photon energy scan between $h\nu$ = 33 eV and $h\nu$ = 120 eV ($\mathbf{k}_\perp \approx 3$ Å$^{-1}$– 5.5 Å$^{-1}$), taken along the $\overline{\Gamma}$-$\overline{K}$ direction at normal emission ($E_B$=100 meV). The spectra have been normalized to have equal intensity for each $\mathbf{k}_\perp$. (c-e) Stacks of experimental constant energy contours at different $E_B$. Red dotted lines are a guides for the eye indicating TSS.

Figure 2(a) shows ARPES data obtained on a 10 nm-thick $\alpha$-Sn film using a photon energy of $h\nu$ = 18 eV. Such photon energy corresponds to a surface perpendicular momentum $\mathbf{k}_\perp = 1.33\times(2\pi/c)$, assuming an inner potential of $V_0$ = 5.8 eV [5] and $c$ = 3.75 Å (interplanar distance in $\alpha$-Sn), which allows to highlight the surface states. The very presence of a well-ordered surface provides good quality ARPES data, while no signature of a (8×8) reconstruction in the electronic structure is observed. The Fermi level is pinned $\sim$ 100 meV below the valence band maximum of the projected bulk bands [Fig. 2(a)], therefore, the expected band gap in the bulk electronic structure defined by quantum confinement [26] is not accessible. Apart from the projected bulk bands that possess 60°-twinned 3-fold character visible in Fig. 2(c-e), the electronic structure of $\alpha$-Sn films harbor an additional pair of linear-like crossing bands with a cross-point $\sim$ 200 meV below $E_F$ [Fig. 2(a)]. The linear-like state has a group velocity of (4.8 ± 0.5) eV Å, i.e., (7.3 ± 0.8) × $10^5$ m/s [see Fig. 3(a)], which agrees well with the previously reported value for $\alpha$-Sn on InSb(001) [2]. However, in contrast to $\alpha$-Sn on InSb(001) and InSb(111)B [13, 18], our data reveals a TSS with a DP located higher in binding energy, which allows to observe the TSS branches below and above the DP. We note that due to the doping level of our $\alpha$-Sn films, as well as the limited ARPES resolution, we are not able to observe (gapped) topological surface states in the meV-range near CB minimum which were recently reported in transport data in HgTe films [36].

The two-dimensional character of the TSS is further experimentally confirmed by measuring ARPES at different photon energies [Fig. 2(b)]. Clearly, the TSS shows no dispersion with varying photon energy ($\mathbf{k}_\perp$ momentum) — except at the photon energies corresponding to the bulk Γ-points in the surface normal direction where the intensity of the bulk bands start to dominate ($\mathbf{k}_\perp$ = 3.3 Å$^{-1}$(2×(2$\pi$/$c$)) and 5.0 Å$^{-1}$(3×(2$\pi$/$c$))). We note that, similar to the case of the (001)-surface, the momentum distribution of the TSS at given binding energies is isotropic in the $\mathbf{k}_\parallel$ plane and does not show any noticeable warping effects [Figs. 2(c-e)].

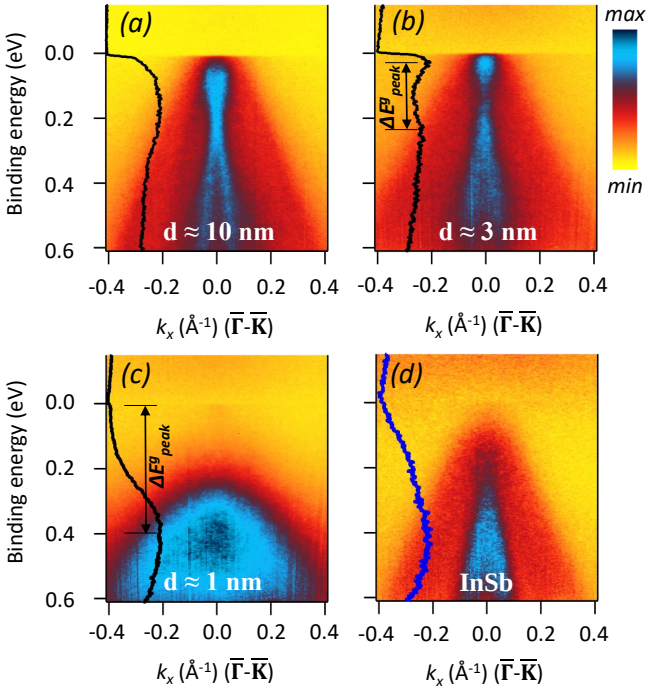


FIG. 3. ARPES band maps as a function of $\alpha$-Sn film thickness. The photon energy was 18 eV and the temperature 8 K. EDCs at normal emission are overlayed on the left of each panel. (a) 10 nm-thick, (b) 3 nm-thick, and, (c) 1 nm-thick $\alpha$-Sn films. (d) Clean InSb(111)A substrate.

The clear visibility of the DP allows for probing the possible opening of a hybridization gap in TSS upon reducing the $\alpha$-Sn film thickness, i.e., to observe a transition from a quasi-3D TI to a quasi-2D TI with gapped TSS. Figure 3 shows ARPES maps for different $\alpha$-Sn film thicknesses. The EDCs taken at the Γ-point are overlayed on the left side of each map. Despite the relatively thin film thickness, the energy distribution curve (EDC) taken through the DP [Fig. 3(a)] does not reveal any hybridization gap in the TSS in a 10 nm $\alpha$-Sn film. We note that the larger energy difference between $s$-like $\Gamma_7^-$ and

$p$-like $\Gamma_8^+$ bands in $\alpha$-Sn, as compared to HgTe, leads to a different critical quantum well thickness below which the bulk band inversion is lost. The electron-like band from the *gapped TSS* was calculated to cross the heavy-hole band in CdTe/$\alpha$-Sn quantum wells at a critical thickness of 2.7 nm [26] (compare to $t_{crit} = 6.3$ nm for HgTe), defining the transition to a 2D trivial state. Recently, the QSHI phase in free-standing $\alpha$-Sn(001) films was calculated for thickness above $d_{crit} \approx 2$ nm [27]. In contrast to CdTe-based and free-standing (vacuum-based) quantum wells, the semiconducting InSb substrate allows for less localized interface-TSS at similar $\alpha$-Sn film thickness, which, in turn, reduces the TSSs hybridization and, therefore, quantum well critical thickness.

With the thickness reduced to 3 nm we observe a slight $p$-doping effect in the electronic structure (energy shift $\Delta E \approx 80$ meV). Such a behavior is consistent with shift of the VB offset of $\sim 100$ meV for thinner $\alpha$-Sn films (determined by XPS; not shown here). The band gap in the projected bulk electronic structure remains unresolved in ARPES as it is still situated above the $E_F$. However, a clear reduction of the spectral weight at the DP is observed for the 3-nm-thick film [Fig. 3(b)]. This is likely a result of the TSS hybridization between the surface- and interface-TSS. However, instead of a well-defined hybridization gap, the corresponding EDC taken at the Γ-point shows a rather broad local minimum at the DP, which could be a combined effect of the background of the projected bulk states and lateral fluctuations in energy positions of the surface- and interface-TSS. The energy difference between the EDC maxima is found to be $\Delta E^g_{peak} \approx 200$ meV , which is again lower than the theoretical value for a CdTe/$\alpha$-Sn quantum well [26]. This discrepancy is most probably due to the more relaxed boundary conditions.

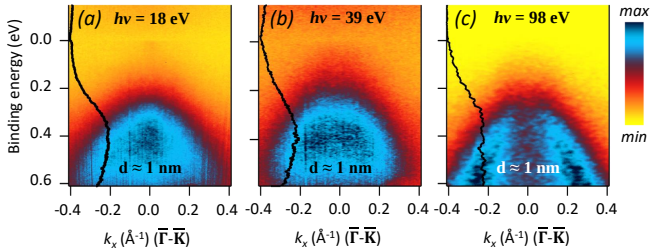


FIG. 4. ARPES data measured on a 1 nm-thick $\alpha$-Sn film at different photon energies $h\nu$ of 18 eV (left), 39 eV (center), and 98 eV (right). EDCs at normal emission are overlayed in each panel.

Reducing the film thickness further, the TSS hybridization becomes stronger. The 1 nm-thick $\alpha$-Sn film reveals a total gap of $\Delta E^g_{peak} \geq 400$ meV [see Fig. 3(c)] since the CB minimum is at or higher than $E_F$. In addition, the bulk electronic structure looses dispersive behavior in $\mathbf{k}_\perp$ due to a strong confinement. This can be seen in Fig. 4 where the $\mathbf{k}_\parallel$-dispersion shows only a minor variation with photon energy. As a consequence, we are not able to distinguish experimentally between hybridized TSS states and quasi-2D bulk states. Note that the measured film data are clearly distinct from those of a clean InSb substrate [Fig. 3(d)]. The quasi-2D character of the bulk electronic structure of the 1 nm-thick film is consistent with the data reported in Ref. [18] for bilayer stanene on InSb(111)B. Nevertheless, our results do not fully agree with the data reported in Refs. [13, 18] for thicker $\alpha$-Sn films since the quantum well and TSS hybridization effects are much more pronounced both in our calculations (see Fig. 5) and in the experimental data.

In order to trace the change of the electronic structure with film thickness we performed DFT calculations. Figure 5 presents the calculation results obtained for 7.1 nm-thick (a,c,e) and 0.75 nm-thick (b,d,f) $\alpha$-Sn films on InSb(111)A, respectively. The blue and red colors in Figs. 5(a-d) denote the spin polarization, while the size of the circles is proportional to the density of states in the first two layers, and above the layers for the 0.75 nm-thick and 7.1 nm-thick films, respectively. Figures 5(c,d) show the enlarged region around $E_F$ comparable to the experimental data presented in Fig. 3.

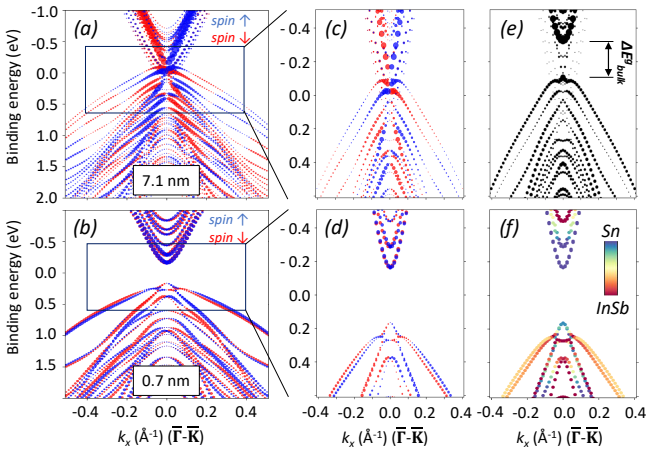


FIG. 5. DFT calculations of a 7.1 nm-thick (a,c,e) and a 0.7 nm-thick (b,d,f) $\alpha$-Sn film on InSb(111)A. (a-d) The blue and red colors denote the spin polarization, while the size of the circles is a measure of the *surface* density of states of the $\alpha$-Sn film. (e) The size of the circles is proportional to the $\alpha$-Sn density of states in the middle of the $\alpha$-Sn film, i.e., *bulk* states. (f) Same as (d), however, here the color indicates the respective contributions from the Sn and InSb states.

For the 7.1-nm-thick $\alpha$-Sn film, the linearly dispersing spin-polarized surface states can be recognized in the electronic structure [Figs. 5(a,c)]. Yet, in contrast to the experimental data, the DP is located in the vicinity of $E_F$ [Fig. 5(c)], which, in turn, is close to the valence band maximum. Apart from this mismatch in the energy position that depends on the alignment of the potentials between the substrate and the $\alpha$-Sn film, the theoretical data agrees well with the experimental TSS shown in Fig. 2(a). The size of the dots in Fig. 5(e) is proportional to the density of states in the middle of the $\alpha$-Sn

film, and thus reveal a quantum confinement gap in the *bulk states* of $\Delta E^g_{bulk} \approx 200\,\text{meV}$. The hybridization gap in TSS (Fig. 5(c)) has much smaller value of $\Delta E^g_{peak} \approx 30\,\text{meV}$.

For the 0.7 nm-thick $\alpha$-Sn film, a gap of $\sim$330 meV in the electronic structure is clearly resolved in calculations [Figs. 5(b,d)], which is smaller than the experimentally determined gap of at least $\sim 400\,\text{meV}$ [Fig. 3(c)]. We note that for such thin $\alpha$-Sn films, the calculated density of states in the first two layers also contain a contribution from the InSb substrate states. However, as can be seen in Fig. 5(f), the calculated gap of $\sim 330\,\text{meV}$ is due to Sn states.

TABLE I. Experimental TSS hybridization gap and theoretical $s$-like and $p$-like bands order near $E_\text{F}$ at $\Gamma$-point as a function of $\alpha$-Sn thickness in $\alpha$-Sn/InSb(111)A system.

| $\alpha$-Sn thickness | TSS gap $\Delta E^g_{peak}$ | Bands order |
|---|---|---|
| $\sim 10\,\text{nm}$ | Not resolved | Inverted |
| $\sim 3\,\text{nm}$ | $\approx$200 meV | Inverted |
| $\sim 1\,\text{nm}$ | $\geq$400 meV | Trivial |

We further check the topological character of $\alpha$-Sn thin films by tracking the relative energy positions of $s$-like and $p$-like bands near $E_\text{F}$ as a function of thickness. The results are listed in Tab. I together with the values of TSS hybridization gap estimated from the ARPES data. For the 7.1 nm-thick films the band order is inverted, i.e., $s$-like minima is below $p$-like maxima. The band inversion remains also in 2.5 nm-thick films where we find that $s$-like band penetrates into the InSb substrate thus enhancing the effective quantum well width. However, in the 0.7 nm-thick $\alpha$-Sn film the $s$-like band position is now *above* the $p$-like band, which is a signature of topologically *trivial* electronic structure. Therefore, the theoretical critical thickness for transition to a trivial 2D insulator $d_{crit}$ is between 0.7 nm and 2.5 nm and can be rouglhy estimated to have a value of $d_{crit} = 1.6\,\text{nm}$. For the $\alpha$-Sn films with thickness more than $d_{crit}$ and less than $\sim 10\,\text{nm}$, the topologically protected 1D chiral edge channels must be present owing to the gap in TSS and inverted electronic band structure.

## IV. CONCLUSIONS

In conclusion, we report on the electronic structure of $\alpha$-Sn films on InSb(111)A grown by MBE and, more importantly, the evolution of the TSS as a function of film thickness. We observe a new (8×8) surface reconstruction, which to the best of our knowledge, was not reported so far. As in case of $\alpha$-Sn on InSb(001), in 10-nm-thick $\alpha$-Sn films the observed TSS is largely degenerate with the bulk band structure. However, the DP was found to be $\sim 200\,\text{meV}$ below the $E_\text{F}$. The latter allows for the observation of the hybridization gap opening in the TSS for thinner $\alpha$-Sn films: in 3-nm-thick $\alpha$-Sn film we determine a gap in the TSS of the order of $\sim 200\,\text{meV}$. The crossover from the 3D to the quasi-2D stanene-like electronic structure in a 1-nm-thick film is accompanied by a full gap opening ($\Delta E^g_{peak} \approx 400\,\text{meV}$) at the $\Gamma$-point in agreement with the calculated few-layer-stanene electronic bandstructure. Our DFT electronic structure calculations of thin $\alpha$-Sn films on InSb(111)A show good agreement with the experimental data, as well as provide evidence for the spin-polarized character of the observed TSS. The latter, however, needs to be verified in future experiments. Furthermore, while we have identified the topologically non-trivial character of $\sim 10\,\text{nm}$- and $\sim 3\,\text{nm}$-thick $\alpha$-Sn films, we find no band inversion in the $\sim 1\,\text{nm}$-thick $\alpha$-Sn film. Therefore, the thickness regime of $\alpha$-Sn films where both the gapped TSS and topologically non-trivial bandstructure coexist is about $\sim 2$ - $10\,\text{nm}$. In this thickness regime, topologically protected 1D chiral edge states must exist, although, not easily accessible due to the overlap with the bulk bands.

## V. ACKNOWLEDGMENTS

This work was supported by the Deutsche Forschungsgemeinschaft (DFG) under Grant SCHA1510/5, the SPP 1666 Priority Program "Topological Insulators", the DFG Collaborative Research Center SFB 1170 "ToCoTronics" in Würzburg. We acknowledge financial support from the DFG through the Würzburg-Dresden Cluster of Excellence on Complexity and Topology in Quantum Matter – *ct.qmat* (EXC 2147, project-id 39085490). Diamond Light Source (Didcot, UK) is gratefully acknowledged for beamtime under proposals SI10244, SI10289, SI12892, and SI15285. LBD acknowledges financial support from EPSRC (UK) and the Science and Technology Facilities Council (UK).

[1] L. Fu and C. L. Kane, Topological insulators with inversion symmetry, Phys. Rev. B **76**, 045302 (2007).

[2] A. Barfuss, L. Dudy, M. R. Scholz, H. Roth, P. Höpfner, C. Blumenstein, G. Landolt, J. H. Dil, N. C. Plumb,

M. Radovic, A. Bostwick, E. Rotenberg, A. Fleszar, G. Bihlmayer, D. Wortmann, G. Li, W. Hanke, R. Claessen, and J. Schäfer, Elemental Topological Insulator with Tunable Fermi Level: Strained $\alpha$-Sn on InSb(001), Phys. Rev. Lett. **111**, 157205 (2013).

[3] Y. Ohtsubo, P. Le Fèvre, F. Bertran, and A. Taleb-Ibrahimi, Dirac Cone with Helical Spin Polarization in Ultrathin $\alpha$-Sn(001) Films, Phys. Rev. Lett. **111**, 216401 (2013).

[4] J. C. Rojas-Sánchez, S. Oyarzun, Y. Fu, A. Marty, C. Vergnaud, S. Gambarelli, L. Vila, M. Jamet, Y. Ohtsubo, A. Taleb-Ibrahimi, P. Le Fèvre, F. Bertran, N. Reyren, J. M. George, and A. Fert, Spin to Charge Conversion at Room Temperature by Spin Pumping into a New Type of Topological Insulator: $\alpha$ -Sn Films, Phys. Rev. Lett. **116**, 096602 (2016).

[5] V. A. Rogalev, T. Rauch, M. R. Scholz, F. Reis, L. Dudy, A. Fleszar, M.-A. Husanu, V. N. Strocov, J. Henk, I. Mertig, J. Schäfer, and R. Claessen, Double Band Inversion in $\alpha$-Sn: Appearance of Topological Surface States and the Role of Orbital Composition, Phys. Rev. B (Rap. Comm.) **95**, 161117 (2017).

[6] H. Huang and F. Liu, Tensile strained gray tin: Dirac semimetal for observing negative magnetoresistance with Shubnikov–de Haas oscillations, Phys. Rev. B **95**, 201101 (2017).

[7] Q. Barbedienne, J. Varignon, N. Reyren, A. Marty, C. Vergnaud, M. Jamet, C. Gomez-Carbonell, A. Lemaitre, P. Le Fèvre, F. Bertran, A. Taleb-Ibrahimi, H. Jaffrès, J.-M. George, and A. Fert, Angular-resolved photoemission electron spectroscopy and transport studies of the elemental topological insulator $\alpha$-Sn, Phys. Rev. B **98**, 195445 (2018).

[8] O. Vail, P. Taylor, P. Folkes, B. Nichols, B. Haidet, K. Mukherjee, and G. de Coster, Growth and Magnetotransport in Thin Film $\alpha$-Sn on CdTe, Physica Status Solidi (b).

[9] Z. Zhu, Y. Cheng, and U. Schwingenschlögl, Band inversion mechanism in topological insulators: A guideline for materials design, Phys. Rev. B **85**, 235401 (2012).

[10] N. Berchenko and M. Pashkovskiĭ, Mercury telluride—a zero-gap semiconductor, Soviet Physics Uspekhi **19**, 462 (1976).

[11] B. Volkov and O. Pankratov, Two-dimensional massless electrons in an inverted contact, JETP Lett **42**, 178 (1985).

[12] S. Chadov, X. Qi, J. Kübler, G. H. Fecher, C. Felser, and S. C. Zhang, Tunable multifunctional topological insulators in ternary Heusler compounds., Nat. mat. **9**, 541 (2010).

[13] C.-Z. Xu, Y.-H. Chan, Y. Chen, P. Chen, X. Wang, C. Dejoie, M.-H. Wong, J. A. Hlevyack, H. Ryu, H.-Y. Kee, N. Tamura, M.-Y. Chou, Z. Hussain, S.-K. Mo, and T.-C. Chiang, Elemental Topological Dirac Semimetal: $\alpha$-Sn on InSb(111), Phys. Rev. Lett. **118**, 146402 (2017).

[14] M. R. Scholz, V. A. Rogalev, L. Dudy, F. Reis, F. Adler, J. Aulbach, L. J. Collins-McIntyre, L. B. Duffy, H. F. Yang, Y. L. Chen, T. Hesjedal, Z. K. Liu, M. Hoesch, S. Muff, J. H. Dil, J. Schäfer, and R. Claessen, The topological surface state of $\alpha$-Sn on InSb(001) as studied by photoemission, Phys. Rev. B **97**, 075101 (2018).

[15] G. Li, Y.-Y. Zhang, H. Guo, L. Huang, H. Lu, X. Lin, Y.-L. Wang, S. Du, and H.-J. Gao, Epitaxial growth and physical properties of 2D materials beyond graphene: from monatomic materials to binary compounds, Chem. Soc. Rev. **47**, 6073 (2018).

[16] F.-F. Zhu, W.-J. Chen, Y. Xu, C.-L. Gao, D.-D. Guan, C.-H. Liu, D. Qian, S.-C. Zhang, and J.-F. Jia, Epitaxial growth of two-dimensional stanene, Nat. Mater. **14**, 1020 (2015).

[17] J. Gou, L. Kong, H. Li, Q. Zhong, W. Li, P. Cheng, L. Chen, and K. Wu, Strain-induced band engineering in monolayer stanene on Sb(111), Phys. Rev. Mater. **1**, 054004 (2017).

[18] C. Z. Xu, Y. H. Chan, P. Chen, X. Wang, D. Flötotto, J. A. Hlevyack, G. Bian, S. K. Mo, M. Y. Chou, and T. C. Chiang, Gapped electronic structure of epitaxial stanene on InSb(111), Phys. Rev. B **97**, 035122 (2018).

[19] Y. Zang, T. Jiang, Y. Gong, Z. Guan, C. Liu, M. Liao, K. Zhu, Z. Li, L. Wang, W. Li, C. Song, D. Zhang, Y. Xu, K. He, X. Ma, S.-C. Zhang, and Q.-K. Xue, Realizing an epitaxial decorated stanene with an insulating bandgap, Adv. Funct. Mater. **28**, 1802723 (2018).

[20] J. Deng, B. Xia, X. Ma, H. Chen, H. Shan, X. Zhai, B. Li, A. Zhao, Y. Xu, W. Duan, S.-C. Zhang, B. Wang, and J. G. Hou, Epitaxial growth of ultraflat stanene with topological band inversion, Nat. Mater. **17**, 1081 (2018).

[21] J. Yuhara, Y. Fujii, K. Nishino, N. Isobe, M. Nakatake, L. Xian, A. Rubio, and G. L. Lay, Large area planar stanene epitaxially grown on Ag(111), 2D Materials **5**, 025002 (2018).

[22] X. Zheng, J.-F. Zhang, B. Tong, and R.-R. Du, Epitaxial growth and electronic properties of few-layer stanene on insb (111), 2D Materials (2019).

[23] B. A. Bernevig, T. L. Hughes, and S.-C. Zhang, Quantum Spin Hall Effect and Topological Phase Transition in HgTe Quantum Wells, Science **314**, 1757 (2006).

[24] M. König, S. Wiedmann, C. Bruene, A. Roth, H. Buhmann, L. W. Molenkamp, X.-L. Qi, and S. C. Zhang, Quantum spin hall insulator state in HgTe quantum wells, Science **318**, 766 (2007).

[25] B.-H. Chou, Z.-Q. Huang, C.-H. Hsu, F.-C. Chuang, Y.-T. Liu, H. Lin, and A. Bansil, Hydrogenated ultra-thin tin films predicted as two-dimensional topological insulators, New Journal of Physics **16**, 115008 (2014).

[26] G. J. de Coster, P. A. Folkes, P. J. Taylor, and O. A. Vail, Effects of orientation and strain on the topological characteristics of CdTe/$\alpha$-Sn quantum wells, Phys. Rev. B **98**, 115153 (2018).

[27] J. Li and Y. Xu, Quantum Spin Hall Insulators in Tin Films: Beyond Stanene, arXiv preprint arXiv:1909.09326 (2019).

[28] C.-X. Liu, H. Zhang, B. Yan, X.-L. Qi, T. Frauenheim, X. Dai, Z. Fang, and S.-C. Zhang, Oscillatory crossover from two-dimensional to three-dimensional topological insulators, Physical review B **81**, 041307 (2010).

[29] A. A. Baker, W. Braun, G. Gassler, S. Rembold, A. Fischer, and T. Hesjedal, An ultra-compact, high-throughput molecular beam epitaxy growth system, Rev. Sci. Instrum. **86**, 043901 (2015).

[30] E. Wimmer, H. Krakauer, M. Weinert, and A. J. Freeman, Full-potential self-consistent linearized-augmented-plane-wave method for calculating the electronic structure of molecules and surfaces: $O_2$ molecule, Physical Review B **24**, 864 (1981).

[31] S. H. Vosko, L. Wilk, and M. Nusair, Accurate spin-dependent electron liquid correlation energies for local spin density calculations: a critical analysis, Canadian

Journal of physics **58**, 1200 (1980).

[32] C. Li, A. J. Freeman, H. Jansen, and C. Fu, Magnetic anisotropy in low-dimensional ferromagnetic systems: Fe monolayers on Ag (001), Au (001), and Pd (001) substrates, Physical Review B **42**, 5433 (1990).

[33] T. Osaka, H. Omi, K. Yamamoto, and A. Ohtake, Surface phase transition and interface interaction in the $\alpha$-Sn/InSb {111} system, Phys. Rev. B **50**, 7567 (1994).

[34] P. Fantini, S. Gardonio, P. Barbieri, U. del Pennino, C. Mariani, M. G. Betti, E. Magnano, M. Pivetta, and M. Sancrotti, $\alpha$-Sn pseudomorphic growth on InSb (111) and ($\underline{111}$) surfaces: a high-resolution photoemission study, Surf. science **463**, 174 (2000).

[35] H. Zimmermann, R. C. Keller, P. Meisen, H. Richter, and M. Seelmann-Eggebert, Interface formation between deposited Sn and $Hg_{0.8}Cd_{0.2}Te$, J. Electron. Mater. **25**, 1293 (1996).

[36] D. M. Mahler, J.-B. Mayer, P. Leubner, L. Lunczer, D. Di Sante, G. Sangiovanni, R. Thomale, E. M. Hankiewicz, H. Buhmann, C. Gould, and L. W. Molenkamp, Interplay of Dirac nodes and Volkov-Pankratov surface states in compressively strained HgTe, Phys. Rev. X **9**, 031034 (2019).